MANUSCRIPT TITLE

Transcription-Coupled Repair of DNA Interstrand Crosslinks by UVSSA

AUTHORS

Rowyn Church Liebau[1], Crystal Waters[2], Arooba Ahmed[2], Rajesh K Soni[3], and Jean Gautier[2,*]

[1] Institute for Cancer Genetics, Graduate School of Arts and Sciences, Columbia University, New York, NY, 10027, United States of America

[2]Institute of Cancer Genetics, Columbia University Irving Medical Center , New York, NY 10032, United States of America

[3]Proteomics and Macromolecular Crystallography Shared Resource, Herbert Irving Comprehensive Cancer Center, Columbia University, New Yor, NY 10032, United States of America

* To whom correspondence should be addressed. Tel: (212) 851-4567; Email: jg130@cumc.columbia.edu

GRAPHICAL ABSTRACT

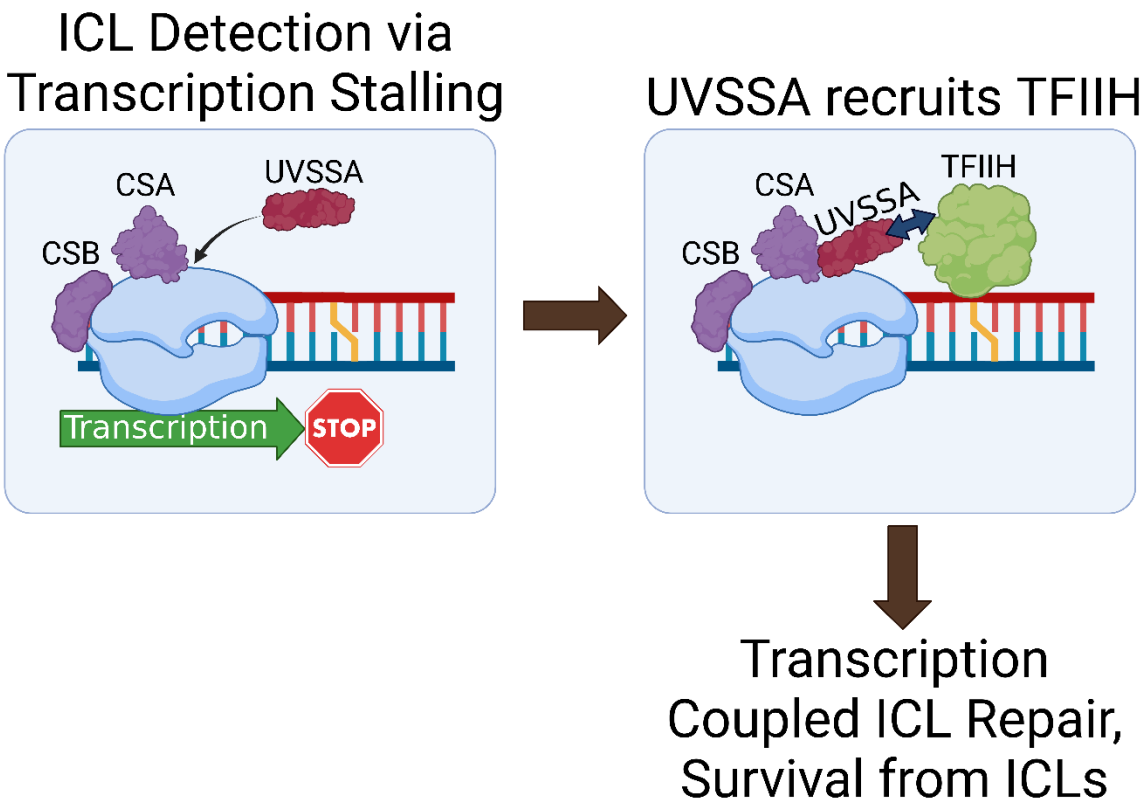

UVSSA facilitates transcription-coupled DNA interstrand crosslink repair by recruiting TFIIH to transcription machinery stalled at the lesion. Transcription-coupled ICL repair is required for survival following crosslink inducing drug exposure

ABSTRACT

DNA interstrand crosslinks (ICLs) are covalent bonds between opposing strands of the DNA helix which prevent DNA melting and subsequent DNA replication or RNA transcription. Here, we show that UV Stimulated Scaffold Protein A (UVSSA) participates in transcription-coupled repair of ICLs. UVSSA encodes a protein that regulates the activity of RNA polymerase II (Pol II) to facilitate the repair of UV lesions and to relieve transcription stress resulting from MYC activation. We show that UVSSA knockout sensitizes cells to ICL-inducing drugs, that UVSSA is specifically required for transcription-coupled repair of a single ICL in a fluorescence-based reporter assay, and that transcription-coupled repair of ICLs is defective in UVSSA$^{-/-}$ cells. UVSSA localizes to chromatin upon ICL damage, and interacts with transcribing Pol II, CSA, CSB, and TFIIH. The UVSSA-TFIIH interaction facilitates ICL repair. Finally, UVSSA expression positively correlates with ICL chemotherapy resistance in cancer cell lines. Our data strongly suggest that transcription-coupled ICL repair (TC-ICR) is a *bona fide* ICL repair mechanism that contributes to crosslinker drug resistance independently of replication-coupled ICL repair.

INTRODUCTION

DNA interstrand crosslinks (ICLs) are DNA lesions characterized by a covalent bond between opposing strands of the DNA helix. DNA crosslinks prevent melting of double stranded DNA, blocking essential DNA transactions including RNA transcription and DNA replication (1). ICLs can be caused by products of endogenous metabolic activity as well as following exposure to chemotherapeutic drugs. Unrepaired ICLs disrupt replication, halt the cell cycle, and trigger apoptosis (2). To preserve genome integrity, organisms have evolved repair mechanisms to remove ICLs.

The best understood ICL repair mechanism is the Fanconi Anemia (FA) pathway. The FA pathway was identified in patients suffering from Fanconi Anemia, an inherited genetic disorder characterized by bone marrow failure, high incidence of early onset cancer, and extreme sensitivity to crosslinking agents. FA patients harbor mutations in one of 23 genes that make up the FA pathway. FA is activated during DNA replication, when a replication fork stalls at an ICL. The stalled fork is recognized by FA proteins, which activate downstream repair mechanisms to effect removal of the lesion and resumption of replication. Cells harboring mutation in the FA pathway are not able to resolve these replication blocks, and accumulate DNA double strand breaks (DSBs) and mutations (1).

Replication-coupled repair by FA is thought to be the major repair mechanism to remove ICLs. However, non-replicative or rarely replicating cells must still repair ICLs to preserve genome integrity. Investigation of replication independent repair (RIR) of ICLs has revealed alternative ICL repair mechanisms that function independently of FA (Reviewed (3)). X*enopus laevis* cell-free extracts which do not undergo replication are still capable of repairing ICLs. RIR requires the DNA polymerase Pol K, implicating translesion synthesis (TLS) in ICL repair outside of replication (4). A component of RIR in *Xenopus* extract is the Mismatch Repair (MMR) protein MutSα, an ICL sensor that detects helix distortion caused by DNA lesions. MutSα initiates repair of ICLs via MMR machinery, allowing for direct detection of the lesion and repair independent of DNA transactions (5). Mammalian cells repair ICLs during G1 via the DNA damage sensor XPC (6). XPC functions in the global genome-nucleotide excision repair (GG-NER) pathway, indicating that multiple repair mechanisms detect and repair ICLs independently of replication (7).

Transcription is another DNA transaction that influences ICL repair. Repair of ICLs is biased towards transcribed regions of the genome (8). Loss of transcription-coupled repair proteins CSA (ERCC8) or CSB (ERCC6) sensitizes cells to drugs that induce crosslinks (9), suggesting that those proteins are required for repair of ICLs. Indeed, CSB was found to promote repair of ICLs during transcription, in conjunction with TLS polymerase Pol ζ (10). Transcription-coupled repair is observed for other DNA lesions, most notably Ultra Violet (UV) light induced base dimers.

Transcription-Coupled Nucleotide Excision Repair (TC-NER) is triggered by lesions that halt transcribing RNA Polymerase II (Pol II), such as UV induced pyrimidine dimers or bulky DNA adducts (11). Pol II stalled at the lesion recruits TC-NER factors CSA, CSB, USP7, and UVSSA to remodel the transcription complex by eviction of DSIF and RFT1 as well as ubiquitylation of RPB1 (12,13). The modified Pol II complex backtracks along the DNA, exposing the lesion for repair. TFIIH is recruited and performs dual endonuclease cleavage, removing the damaged DNA segment from the transcribed strand. Gap filling synthesis and subsequent ligation then restores the transcribed strand (see for review (14,15)).

Mutations in NER genes result in several inherited conditions that are primarily characterized by sensitivity to UV light. Xeroderma Pigmentosum (XP) is caused by mutation in genes XPA-XPG and XPV, resulting in severely increased risk of skin cancer in sun exposed areas. Neurological degeneration also occurs in a minority of patients (16). Cockayne Syndrome (CS), caused by mutation in CSA or CSB coding genes (ERCC8, ERCC6), is characterized by impaired TC-NER, stunted development, severe neurological impairment, and short lifespan. Finally, the relatively mild UV

Sensitivity Syndrome (UVSS) triggers the same UV sensitivity without the cancer predisposition or developmental delays observed in other NER deficiencies (17,18).

UVSS is caused by mutations in the Ultra Violet Stimulated Scaffold-A (UVSSA) protein. UVSSA is recruited to stalled Pol II by CSA (19), and in turn facilitates the recruitment of the USP7 deubiquitinase and TFIIH to stalled Pol II. Loss of UVSSA impairs TC-NER and sensitizes cells to UV damage (20,21). UVSSA also preserves genome stability during oncogene-driven transcriptional stress. We identified UVSSA in a genome-wide screen for genes regulating fitness of cMYC overexpressing cells. UVSSA knockdown sensitizes cells to cMYC overexpression, triggering transcription-dependent synthetic sickness. UVSSA regulates Pol II dynamics during cMYC induced transcriptional stress (22) indicating the importance of the protein for regulation of transcription during genomic stress.

UVSSA was independently identified in two genome-wide screens for genes contributing to survival following ICL damage. Loss of UVSSA sensitized cells to the ICL inducing drugs maphosphamide (23) and cisplatin (24). Given UVSSA's role in transcription-associated genome maintenance, these results suggest that UVSSA functions in Transcription-Coupled ICL Repair (TC-ICR).

Here we show that UVSSA promotes TC-ICR. UVSSA knockout sensitizes cells to crosslinking drugs. Survival following ICLs is mediated by UVSSA binding to TFIIH. Repair of crosslinker induced DNA damage is significantly delayed in UVSSA$^{-/-}$ cells. Using an ICL specific reporter assay, we show that UVSSA is a TC-ICR factor. Finally, we characterize the UVSSA interactome following ICL damage and document the overlap between UV and ICL dependent UVSSA interactions.

MATERIAL AND METHODS

Cell culture

Cells were cultured at 37°C with 5% CO_2. Hap-1 cells (Horizon C631) were cultured in IMDM (Thermo Fisher Scientific) supplemented with 10% FBS (Fisher Scientific) and 1% Penicillin/ Streptomycin (Invitrogen). MCF10a cells (ATCC CRL-10317) were cultured in DMEM/F12 media (Thermo Fisher Scientific) with 5% Horse serum (Invitrogen), 1% Penicillin/Streptomycin, 20µg/ml EGF (Peprotech AF-100-15), 500ug/ml Hydrocortisone (Sigma-Aldrich H0888-1G), 100µg/ml Cholera toxin (Sigma-Aldrich C8052), and 10mg/ml Insulin (Sigma-Aldrich I0516). 293T cells (ATCC CRL-3216) were cultured in DMEM (Thermo Fischer Scientific) supplemented with 10% FBS and 1% Penicillin/ Streptomycin

Clonogenic assay

Cells were seeded at a density of 500 cells per 10cm dish, in triplicate for each condition. Cells were allowed to grow for 24 hours before addition of drugs. After a 4-hour treatment, the medium was removed by aspiration and replaced with fresh medium. Cells were incubated for 7-14 days and stained upon sufficient colony growth. Colonies were fixed in 100% methanol for 5 minutes, followed by stain with 0.5% Crystal Violet for 5 minutes. Plates were rinsed and dried, and colonies were counted using the ICY software or manual counting

Immunofluorescence microscopy

Wildtype and UVSSA$^{-/-}$ MCF10a cells were cultured on 8-well chamber slides and subjected to 20 nM SJG-136 treatment (MedChem Express: HY-14573) or vehicle for 1 hour and incubated at 37 C for either 24, 48, or 72 hours. Cells were washed with PBS once and then pre-extracted with cold 2% PBS-Triton X-100 for 90 seconds. Cells were then washed with cold PBS for 1 minute and then fixed with 4% PFA (Electron Microscopy Sciences: 157-4) for 10 min. Cells were washed with room temperature PBS for 5 minutes before permeabilization in 0.1% PBS-Triton X-100 for 10 min. Cells

were then washed with PBS three times for 5 minutes each before incubation with blocking buffer (3% BSA in PBS-Tween 20) at room temperature for 1 hour. Cells were then incubated overnight at 4°C with primary RPA antibody (Abcam: ab2175, 1/250) diluted in blocking buffer under a Hybrislip (Invitrogen: H-18202). Following primary antibody staining overnight, hybrislip was removed and cells were washed with PBS for 5 minutes, three times. Cells were then incubated with Alexa 488 conjugated goat anti-mouse IgG (Abcam: ab150113, 1/1,000) secondary antibody and DAPI stain (Invitrogen, 1/10,000) diluted in PBS for 1 hour. Following incubation, cells were washed with PBS three times for 5 minutes in the dark. Slides were prepared using Vectashield Mounting Medium (Vector Laboratories: H-1000-10) and then coverslipped.

Slides were analyzed under 40x magnification using a Zeiss Axio Imager Z2 microscope, equipped with a CoolCube1 camera (Carl Zeiss). MetaCyte software (version 3.10.6) was used to detect nuclei stained with DAPI and to perform automated foci quantification with customized classifiers. For each time point, a minimum of 300 cells were analyzed.

Protein whole cell lysis preparation

For whole cell lysates, cells were lysed in RIPA lysis buffer (NaCl 150mM, NP-40 1%, Deoxycholate 0.5%, Sodium Dodecyl Sulfate 1%, Tris HCl pH 8 50mM) 30 minutes on ice followed by high-speed centrifugation and collection of the supernatant. Protein concentration was quantified using the Pierce BCA Protein Assay Kit (Thermo Scientific 23225). Lysates were mixed with equal volume 2x Laemmli buffer (Sodium Dodecyl Sulfate 4%, 2-mercaptoethanol 10%, glycerol 20%, Bromophenol Blue 0.004%, Tris HCl pH 8 125mM) and boiled for 5 minutes at 95°C before storage at -20°C

Chromatin fractionation

Cells were fractionated as described in (19). Briefly, cells were lysed in fractionation buffer (Tris HCl pH 7.5, KCl 100mM, Sucrose 300mM, $MgCl_2$ 2mM, Triton 0.1%, $CaCl_2$ 1mM, Dithiothreitol 1mM) on ice for 10 minutes, followed by centrifugation 5 min 3800 xG at 4°C. The supernatant was collected and saved as the soluble fraction. The pellet was washed in buffer, followed by digestion with Micrococcal Nuclease in buffer at 1000 units/ml for 30 minutes at room temperature. Digestion was halted by addition of ethylenediaminetetraacetic acid to a final concentration of 5mM. Samples were centrifuged 5 min 3800 xG at 4°C and the supernatant was collected. The pellet was washed with fractionation buffer and centrifuged again, and the supernatants were combined to generate the chromatin fraction. Protein concentration was assayed by BCA as above, and lysates were then boiled in equal volumes 2x Laemmli buffer before storage at -20°C

Western blotting

Samples were run on precast Tris-Glycine 8% Novex gels (Thermo Fisher Scientific XP00080BOX) with GTS running buffer (Tris 25 mM, Glycine 190 mM, SDS 0.1%) or 4-12% Bis-Tris precast NuPAGE gels (Thermo Fisher Scientific NP0322BOX) with MOPS running buffer (Thermo Scientific NP0001). For whole cell lysates, 60µg of protein was loaded. For cellular fractions, 60µg or 30µg of protein was loaded for the soluble or chromatin fractions, respectively. Proteins were transferred to PVDF membrane using the Iblot 2 system (Thermo Fisher Scientific IB21001). Membranes were then blocked for 1-2 hours in 5% powdered milk in PBST. Membranes were incubated overnight at 4°C with diluted antibodies as indicated. Membranes were then washed in PBST for 5 minutes 4X, followed by incubation with appropriate HRP conjugated secondary antibody at 1:10000-1:50000 dilution for 1 hour at room temperature. Membranes were again washed in PBST 4X 5 minutes each, followed by chemiluminescence either with Peirce ECL western Blotting Substrate (Thermo Fisher Scientific 32106), SuperSignal West Pico Plus (Thermo Fisher 34580), or SuperSignal West Dura extended Duration Substrate (Fisher Scientific 37071)

Co-Immunoprecipitation

Cellular fractions generated following chromatin fractionation protocol were pre cleared by mixing with Sepharose beads (Sigma-Aldrich 4B200) for 30 minutes at 4°C. After centrifugation, the supernatant was extracted using a 30-gauge needle, and then incubated with Anti-Flag M2 affinity gel (Sigma-Aldrich A2220) overnight at 4°C. Beads were washed 5x steps in fractionation buffer, then proteins were eluted in 2x SDS sample buffer (Tris HCl pH 6.8 125 mM, SDS 4%, Glycerol 20%, Bromophenol Blue 0.004%) by boiling at 95°C. 5-10ul of elution sample was ran for western blot.

Western blot quantification

Quantification was performed using ImageJ software. The mean gray value for each band was evaluated and processed to correct for background signal. This value was then normalized to loading control signal. The band intensity was then normalized to the average of untreated samples, if detectable.

On-beads digestion for mass spectrometry

The Co-IP protocol above was followed until completion of the final wash step. Immunoprecipitated proteins on agarose beads were then washed five times with 200 µl of 100 mM Tris-pH 8.0. Proteins were reduced with 10 mM TCEP and alkylated with 11 mM iodoacetamide (IAA) that was quenched with 5 mM DTT. Protein digestion was processed by adding 1 µg of trypsin/Lys-C mix and incubated overnight at 37°C and 1400 rpm in a thermomixer. The next day, digested peptides were collected in a new microfuge tube and digestion was stopped by the addition of 1% TFA (final v/v), followed by centrifugation at 14,000 x g for 10 min at room temperature. Cleared digested peptides were desalted on an SDB-RPS Stage-Tip (25), and dried in a speed-vac. Peptides were dissolved in 3% acetonitrile/0.1% formic acid.

Liquid chromatography with tandem mass spectrometry (LC-MS/MS)

Peptides were separated within 80 min at a flow rate of 400 nl/min on a reversed-phase C18 column with an integrated CaptiveSpray Emitter (25 cm x 75µm, 1.6 µm, IonOpticks). Mobile phases A and B were with 0.1% formic acid in water and 0.1% formic acid in ACN. The fraction of B was linearly increased from 2 to 23% within 70 min, followed by an increase to 35% within 10 min and a further increase to 80% before re-equilibration. The timsTOF Pro was operated in PASEF mode (26) with the following settings: Mass Range 100 to 1700m/z, 1/K0 Start 0.6 Vs/cm-2, End 1.6 Vs/cm-2, Ramp time 100ms, Lock Duty Cycle to 100%, Capillary Voltage 1600V, Dry Gas 3 l/min, Dry Temp 200°C, PASEF settings: 10 MS/MS Frames (1.16 seconds duty cycle), charge range 0-5, an active exclusion for 0.4 min, Target intensity 20000, Intensity threshold 2500, CID collision energy 59eV. A polygon filter was applied to the m/z and ion mobility plane to select features most likely representing peptide precursors rather than singly charged background ions.

LC-MS/MS data analysis

Acquired PASEF raw files were analyzed using the MaxQuant environment V.2.1.3.0 and Andromeda for database searches at default settings with a few modifications (27). The default is used for the first search tolerance and main search tolerance (20 ppm and 4.5 ppm, respectively). MaxQuant was set up to search with the reference human proteome database downloaded from UniProt. MaxQuant performed the search trypsin digestion with up to 2 missed cleavages. Peptide, site, and protein false discovery rates (FDR) were all set to 1% with a minimum of 1 peptide needed for identification; label-free quantitation (LFQ) was performed with a minimum ratio count of 1. The following modifications were used for protein identification and quantification: Carbamidomethylation of cysteine residues (+57.021 Da) was set as static modifications, while the oxidation of methionine residues (+15.995 Da), and deamidation (+0.984) on asparagine were set as a variable modification. Results obtained from MaxQuant, protein groups table was further used for data analysis.

CoIP protein enrichment analysis

LFQ values were extracted from MaxQuant analysis and further analyzed using Perseus software. Standard transformation including removal of "only identified by site" results and transformation by log_2 was performed. Proteins displaying partial detection in one condition (mix of zeros and values) were eliminated, such that only proteins that were consistently detected or not detected remained. Zeros were replaced by imputation from a normal distribution (width 0.3, downshift 1.8) using built in Perseus tools. Finally, significance of enrichment was analyzed using students *t*-test comparing mock treated samples to SJG or UV damaged samples. FDR was calculated using Benjamini-Hochberg method. Log_2 FC was calculated by taking the average of Log_2(LFQ) for each condition and subtracting untreated from treated.

DNA interstrand crosslinked oligonucleotide preparation

Single stranded insert oligonucleotides (see oligo table) were brought to 95°C for 5 minutes and allowed to cool and anneal for 2 hours. 100µg of annealed oligo was mixed with 2x SJG buffer (Triethanolamine 50mM, EDTA 2mM) and SJG-136 was added to a final concentration of 100µM. Oligos were incubated overnight at 37°C before ethanol precipitation. The oligo was then run on a 15% PAGE urea denaturing gel to separate crosslinked from un-crosslinked species. The heavier running crosslinked species was excised from the gel via UV shadowing and then eluted by crush and soak method and isopropanol precipitation. The crosslink bearing oligo and an uncrosslinked control was then phosphorylated by PNK (New England Biolabs M0201S).

pmEmerald-n1 modification for ICL reporter assay

The pmEmerald-n1 plasmid was mutagenized to disrupt the Blp1 site at 1358 and to remove the SV40 replication site using two rounds of Quikchange II site directed mutagenesis (Aligent Technologies 200523). The reporter was digested using Bam HI and Nhe I to insert a fragment from the pEGFP-N3-ΔSV40 plasmid (4) containing two BbsI sites, such that digestion with BbsI would generate overhangs compatible with insertion of a single crosslink bearing oligonucleotide. The resulting plasmid was dubbed pEm-N1-CW. Editing was confirmed by sequencing.

ICL reporter backbone preparation

pEm-n1-CW was digested by BbsI. The digest was run on an ethidium bromide agarose gel and the linearized fragment excised under brightfield light. The linear DNA backbone was then extracted from the gel via electroelution in D-tubes (EMD Millipore 71508-3), followed by phenol chloroform extraction and butanol concentration.

ICL reporter ligation and purification

pEm-n1-CW backbone was ligated to either crosslinked insert or control insert by T4 DNA ligase for 72 hours at 4°C. After confirming ligation by agarose gel electrophoresis, both reporters were purified by phenol chloroform extraction and concentrated by butanol extraction. The crosslink bearing reporter was then digested overnight with BglII Ito remove any un-crosslinked species. Both reporter plasmids were then purified via CsCl gradient to remove linear products and desalted and concentrated using an amicon ultra filter tube (EMD Millipore UFC503024)

ICL reporter transfection

Cells were transfected using the neon transfection system. Following the neon transfection protocol, $3*10^5$ Hap-1cells or $2*10^5$ MCF10a cells were transfected with 1ug pCAGGS carrier DNA, 50ng pmCherry-c1 for transfection efficiency control, and 50ng of either crosslinked or uncrosslinked control reporter. Cells were grown for 24 hours and then collected by trypsinization and

resuspended in PBS before fluorescence acquisition on an Attune NxT Flow Cytometer (Thermo Fischer A29002) and gated for green (530/30 nm) and red (620/15 nm) emission.

ICL repair efficiency calculation

After standard gating to remove doublets, fluorescence gates were set based on a negative control to determine the percentage of cells fluorescing. The mEmerald fluorescing cell population was then subdivided based on fluorescence intensity into low, medium, and bright fluorescing groups. The percentage of cells that fell into the bright intensity gate was then calculated, and normalized to transfection efficiency (calculated from mCherry fluorescence). The normalized bright value of cells transfected with the crosslinked reporter was then divided by the same value for the cell transfected with the control reporter, generating a repair efficiency value. Any technical repeats were averaged. Repair efficiency was then normalized to wild type.

UVSSA knockout by iSTOP

The iSTOP sgRNA was designed using the web tool provided by Dr. Ciccia's lab (https://www.ciccialab-database.com/istop/#/). The sgRNA guide was ligated into the B52 sgRNA expression plasmid. A plasmid expressing the BE3 enzyme, a modified Cas9 enzyme, and containing a blasticidin resistance marker, as described in (28), was generously provided by the Ciccia lab. The BE3 expression vector and the sgSTOP expression vector were cotransfected via JetPEI (Polyplus 101000053) and cells were incubated for 72 hours before selection with blasticidin. The selected population was expanded to generate an uncloned population that was subsequently used for cloning to isolate cells containing the edit. Successful editing was confirmed by RFLP, sequencing, and western blot analysis.

Single cell cloning

Uncloned populations were collected by trypsinization. The suspension was then diluted to a concentration of 4.8 cells per milliliter. 200ul of this suspension was distributed into each well of a 96 well plate. Cells were incubated for 2-3 weeks before identifying single colonies, which were expanded as needed. iSTOP editing was again confirmed by RFLP analysis, sequencing, and western blot for protein expression.

UVSSA mutagenesis

The FLAG-UVSSA fusion protein expressing plasmid (pcDNA3.1 FLAG-UVSSA) was a generous gift from the Tanaka lab. Mutations in UVSSA functional residues were induced using the Q5 mutagenesis system. Primers were designed using the NEB base changer portal (https://nebasechanger.neb.com). Mutation was confirmed by sequencing. The mutated UVSSA coding region was then amplified using primers designed to add AscI and EcoRI restriction sites, allowing ligation into the pBabe-puro backbone for retroviral transduction.

Retroviral transduction

293T cells were transfected with pBabe puro plasmid containing either a wild type or mutated FLAG-UVSSA construct, along with VSV-G and pUVMC packaging plasmids via Jetpei (VWR 89129-916). 293T cells were grown for 24 hours before replacing the media with target cell media. After 24 hours the viral media was collected and filtered through a 0.45 micron filter before being added to cells along with 1 ml of fresh media and polybrene to a final concentration of 10ug/ml. 72 hours after transduction cells were selected with puromycin at a concentration of 2ug/ml. Cells were grown for 48 hours under selection before removal of the antibiotic and expansion of the population for cloning.

Statistical Analyses

Statistical significance of RPA foci counts was calculated using one way ANOVA with multiple comparisons in Graphpad Prism 9 software. Data was gathered from 3 biological replicates with N>300 for each datapoint. All other statistical values presented in the figures were calculated by appropriate *t*-test (paired, unpaired, two tail). Clonogenic survival data was gathered from 6 biological replicates per condition, N=6. ICL repair efficiency data was gathered from 3 independent biological replicates, with any technical repeats averaged, N=3. Western blot band intensity quantification was gathered from 3 biological replicates per condition, N=3. For protein enrichment, significance was analyzed by Perseus software (https://maxquant.net/perseus/) by *t*-test with multiple comparison correction by Benjamini-Hochberg method. CoIP protein enrichment data was collected from 3 independent biological replicates. All other comparisons were analyzed using Graphpad Prism 9 software (https://www.graphpad.com/). Linear regression analysis of DepMap data (table1) was generated by the DepMap web portal (https://depmap.org/portal/), all other regressions were analyzed by Graphpad Prism 9 software. A confidence interval of 95% (P<0.05) was set for all comparisons

Reagents

Primary Antibodies: UVSSA (Genetex GTX106751), Vinculin (Cell signaling Technology 4650S), FLAG M2 (EMD millipore F3165), Pol IIo (EMD millipore 04-1571), CSA (Abcam ab137033), CSB (Santa Cruz Biology sc-166042), Histone 3 (Cell Signaling Technology 9715), HDAC1 (Abcam ab109411), RPA (Abcam ab2175).

Restriction enzymes: all restriction enzymes acquired from NEB: BbsI (R0539S), BamHI (R0136S), NheI-(HF R3131S), BglII (R0144S), AscI (R0558S), EcoRI (R0101S)

Kits: Q5 mutagenesis kit NEB (E0554S)

Equipment: Attune NXT flow cytometer (Thermo fisher scientific A29002). Neon transfection system (Thermo Fischer MPK5000).

Biological Resources

Human cell lines: Hap-1 (Horizon C631), UVSSA^{-} (Horizon HZGHC005817c010). MCF10a (ATCC CRL-10317). 293T (ATCC CRL-3216).

Plasmid vectors: pmEmerald-n1 (Addgene 53976), pBabe-puro (Addgene 10668), pCaggs (BCCM LMBP 2453), pMcherry-c1 (Addgene 58476), B52 (Addgene 100708), VSV-g (Addgene 8454), pUVMC (Addgene 8449)

Websites and programs

iSTOP sgRNA database https://www.ciccialab-database.com/istop/#/ (28). Depmap cancer dependency database https://depmap.org/portal/. NEB base changer mutagenesis PCR design tool https://nebasechanger.neb.com. Perseus protein quantification software, https://maxquant.net/perseus/ (29). FCS express fcs file explorer 7, https://denovosoftware.com/. Graphpad prism 9, https://www.graphpad.com/. ICY bioimaging analysis https://icy.bioimageanalysis.org/. FIJI image processing software https://imagej.net/software/fiji/. (30).

RESULTS

UVSSA loss sensitizes cells to DNA crosslinking drugs and delays crosslinker damage repair

UVSSA was identified in a genome wide CRISPR knockout screen in Acute Lymphocytic Leukemia (ALL) cells as a potential regulator of maphosphamide sensitivity ((23), table S1). Loss of UVSSA resulted in enhanced crosslinking drug sensitivity, suggesting that UVSSA is required for ICL repair, possibly in a transcription-coupled mechanism. We sought to test this idea in UVSSA knockout haploid Hap-1 cells (Fig S1A). We compared the sensitivity of Hap-1 wild type (WT) and UVSSA deficient ($UVSSA^{-}$) cells to ICL inducing drugs cisplatin and mitomycin C (MMC) in clonogenic assays. We observed that $UVSSA^{-}$ cells display significant sensitivity to cisplatin (Fig1A) and MMC (Fig S1b).

To confirm that increased drug sensitivity was due to the loss of the UVSSA protein, we expressed FLAG-UVSSA WT in $UVSSA^{-}$ cells. Following retroviral-mediated expression of FLAG-UVSSA, we isolated $UVSSA^{-}$ lines stably expressing FLAG-UVSSA (fig S1C) (Methods). Expression of FLAG-UVSSA WT restored $UVSSA^{-}$ cisplatin sensitivity to WT levels (Fig 1B). These results establish that UVSSA promotes survival following exposure to ICL inducing drugs.

We also generated a $UVSSA^{-/-}$ line in MCF10a (diploid) cells, a non-transformed epithelial breast cell line. We utilized CRISPR based iSTOP mutagenesis (28). We expressed a nuclease-dead Cas9 fused to APOBEC1 along with a guide RNA to generate a W347* mutation in the UVSSA sequence (Methods). Mutation was confirmed by RFLP analysis and sequencing, and loss of expression was confirmed by western blot (Fig S1A). As anticipated, $UVSSA^{-/-}$ MCF10a cells are also sensitive to cisplatin (Fig 1C).

We reasoned that UVSSA could participate in ICL repair. UVSSA plays a role in repair of UV damage together with the TC-NER pathway (31,32). UVSSA recruits repair factor TFIIH via interaction with residues F408 and V411. Mutation in these residues blocks TFIIH binding and impairs transcription-coupled repair (21). We sought to assess whether the UVSSA-TFIIH interactions were similarly required for UVSSA dependent ICL repair. We generated a FLAG-UVSSA F408A/ V411A coding sequence (Fig S1D), ligated it into a retroviral vector, and subsequently isolated MCF10a $UVSSA^{-/-}$ cell lines expressing the exogenous wild type and mutant FLAG-UVSSA protein at similar levels (Fig S1E). Expression of TFIIH binding deficient, F408A/ V411A, UVSSA only partially rescues cisplatin sensitivity. This suggests that UVSSA-TFIIH interaction is required for survival of crosslinking drugs (Fig1C).

We hypothesized that drug sensitivity might be due to a defect in ICL repair. DNA lesions induced by crosslinking agents can be visualized as damage foci using immunofluorescence microscopy. We sought to monitor the kinetics of Replication Protein A (RPA) foci following treatment with a DNA crosslinker (33-36).

We treated MCF10a WT and $UVSSA^{-/-}$ cells with drug SJG-136, a rationally designed crosslink inducing drug with significant cancer toxicity and rapid ICL formation (37), for one hour and measured RPA foci formation at 24 hour intervals for 3 days (Fig 1D,E). Quantification of RPA foci demonstrated that WT cells averaged very few foci in the untreated control. As anticipated, SJG-136 treatment resulted in a significant increase in RPA foci in both WT and $UVSSA^{-/-}$ cells (compare Fig 1E, columns 1and 3, 2 and 4). By 72 hours however, the average number of foci per cell had returned to control (untreated) levels in WT cells (Fig 1D, columns 1 and 7), reflecting DNA damage repair. In

contrast, RPA foci were still significantly elevated in UVSSA$^{-/-}$ cells (Fig 1E, column 8). The persistence of RPA foci in SJG-136 treated UVSSA$^{-/-}$ cells at 72 hours indicates a defect in repair of SJG-136 induced damage. This strongly suggests that UVSSA plays a role in repair of ICLs and that chemotherapeutic sensitivity observed in UVSSA$^{-/-}$ cells is due to a defect in ICL repair.

Our data indicate that UVSSA contributes to ICL repair. We next sought to confirm that UVSSA facilitates repair of ICLs through a transcription-coupled mechanism.

UVSSA functions in transcription-coupled ICL repair

We designed a reporter plasmid-based assay to specifically assess transcription-coupled repair of a single ICL lesion. The plasmid harbors an ICL-containing oligonucleotide inserted between a CMV promoter and the mEmerald coding sequence. The ICL is induced by the drug SJG-136, which was chosen for convenient chemistry, sequence specificity, and crosslinking efficiency (37). Upon transfection into cells, mEmerald is not expressed unless the lesion is repaired. mEmerald associated fluorescence is quantified to calculate repair efficiency (Fig 2A and Methods). Similar assays have previously been used to measure replication independent ICL repair (4,10,38). The reporter plasmid lacks an origin of replication; thus, the readout is independent of replication and specific to transcription-coupled repair.

We transfected Hap-1 WT, UVSSA^{-}, and UVSSA^{-} cells expressing FLAG-UVSSA with the reporter. UVSSA loss reduced ICL repair efficiency by 50% in UVSSA^{-} cells. Expression of FLAG-UVSSA in UVSSA^{-} cells restored repair efficiency to WT levels (Fig2B), confirming that the phenotype was caused by loss of UVSSA. Our results establish that UVSSA participates in transcription-coupled ICL repair (TC-ICR).

To test the role of the UVSSA-TFIIH interaction in ICL repair, we transfected MCF10a WT, UVSSA$^{-/-}$, and UVSSA$^{-/-}$ cells stably expressing WT or FLAG-UVSSA F408A/V411A with the ICL repair reporter plasmid. Similar to earlier results, TFIIH binding deficient UVSSA was unable to rescue the repair defect, confirming that the UVSSA-TFIIH interaction is required for TC-ICR (Fig 2C).

Our results indicate that UVSSA is required for repair of ICLs that block transcription and strengthen the idea that a replication independent ICL repair pathway involving UVSSA is required for cell survival of crosslinking drugs**.** We next sought to characterize the mechanisms of UVSSA mediated TC-ICR by analyzing UVSSA localization and protein interactions induced by ICL damage.

UVSSA interacts with transcribing Pol II and transcription-coupled repair factors during TC-ICR

We hypothesized that UVSSA may localize to ICL-induced lesions and be enriched on chromatin upon ICL damage. Thus, we fractionated UVSSA^{-} Hap-1 cells expressing FLAG-UVSSA treated with SJG-136 or vehicle. We then probed chromatin and soluble fractions for FLAG-UVSSA (see Methods) by western blot. We found that FLAG-UVSSA localizes to chromatin upon SJG-136 treatment (Fig 3A, quantified Fig S2a).

We next examined UVSSA interaction with RNA polymerase (Pol II) via co-immunoprecipitation (CoIP). UVSSA^{-} Hap-1 cells expressing FLAG-UVSSA WT were treated with SJG-136, fractionated, and anti-FLAG M2 affinity gel was used to isolate FLAG-UVSSA-bound proteins in chromatin fractions. The presence of Pol II was probed using an antibody specific to the RPB-1 subunit phosphorylated at

serine 2, which is specific to elongating Pol II: termed Pol IIo (39). SJG-136 treatment triggered the appearance of a Pol IIo band, indicating that UVSSA interacts with transcribing Pol II upon ICL damage (Fig 3B, quantified fig S2B). UVSSA-Pol IIo interaction was specific to the chromatin fraction (Fig S2C). UVSSA-Pol IIo interaction was also induced by another crosslinking agent, MMC, and by UV irradiation (Fig S2D), as previously described for TC-NER (32). Our results strongly suggest that UVSSA interacts with transcribing Pol II to facilitate TC-ICR.

These data suggest analogous roles for UVSSA in transcription-coupled UV and ICL damage repair, and further supports that TC-ICR is distinct from replication-coupled ICL repair. Therefore, we sought to compare the UVSSA interactomes following SJG-136 treatment or UV irradiation. We immunoprecipitated FLAG-UVSSA from chromatin fractions of mock treated, SJG-136 treated, or UV irradiated Hap-1 UVSSA$^-$ cells expressing FLAG-UVSSA, followed by mass spectrometry (MS). We find that UVSSA interacts with a large set of overlapping partners following ICL or UV damage. Comparison of enrichment values upon UV or SJG-136 damage reveals a significant positive correlation between damage-induced UVSSA interacting proteins (fig 3C). These findings point to a functional similarity between UVSSA ICL and UV damage response, which could indicate a common DNA lesion detection step in TC-NER and TC-ICR.

SJG-136 treatment induced interactions between UVSSA and transcription-coupled repair proteins CSA (ERCC8) and CSB (ERCC6), as well as several TFIIH components (GTF2H4, ERCC3) (fig 3D), suggesting that CSA and CSB also play a role in ICL repair. To test this, we examined CSA and CSB localization in SJG-136 treated Hap-1 cells. We observed that both proteins are enriched on chromatin upon ICL damage. Chromatin localization occurs in both UVSSA$^-$ and FLAG-UVSSA expressing cells (fig 3E, quantified Fig S2E,F), indicating that CSA and CSB localize to chromatin independently of UVSSA. ICL induced CSA and CSB chromatin localization is accompanied by depletion from the soluble fraction (Fig 3E, quantified S2G) as previously observed upon UV damage (40). Notably, CSA depletion from the soluble fraction is more pronounced in UVSSA$^-$ cells than in FLAG-UVSSA expressing UVSSA$^-$ Hap-1 cells (Fig S2G) which may be a consequence of ICL repair failure. Next, we confirmed FLAG-UVSSA interaction with CSA upon ICL damage by Co-IP, (fig 3F) confirming our MS results.

Altogether, our data identify UVSSA as a key protein in TC-ICR. We thus postulated that UVSSA expression levels could influence cancer cell resistance to crosslinking therapies, as overexpression of repair factors has previously been linked to chemoresistance (41,42). We compared UVSSA expression and crosslinker drug resistance of cancer cell lines from the CCLE using DepMap cancer dependency database (depmap.org). We observed a significant positive correlation between UVSSA mRNA levels and cisplatin resistance in several cancer cell types, including Acute Lymphoblastic Leukemia (fig 3G), breast ductal carcinoma, and esophageal lineage cancers. A similar correlation was observed between MMC resistance and UVSSA expression in the same cell types (table 1). Our results suggest that chemoresistance to crosslinking drugs could arise in part via UVSSA-dependent activation of the TC-ICR pathway.

DISCUSSION

DNA ICLs are cytotoxic lesions that arise as consequences of endogenous metabolism or are induced by chemotherapeutic drugs. ICLs covalently link opposing strands of the DNA helix, preventing melting and subsequent DNA transactions including replication and transcription (43). Replication-coupled repair of ICLs requires the FA pathway (44). Replication independent repair (RIR) of ICLs may engage the Mismatch Repair (MMR) pathway (5), Global Genome-Nucleotide Excision Repair (GG-NER) (6) or transcription-coupled repair as reported in the context of CSB (10). Here we identify UVSSA as a key player in transcription-coupled ICL repair (TC-ICR).

UVSSA is required for transcription-coupled ICL repair

We establish that UVSSA participates in ICL repair. First, UVSSA loss sensitizes cells to ICL inducing drugs cisplatin and mitomycin C. Second, UVSSA is required for timely DNA damage repair in cells treated with the crosslinking agent SJG-136. Third, UVSSA is required for ICL repair during transcription in a fluorescence-based reporter assay. Finally, UVSSA expression correlates with crosslinker resistance in several cancer types.

TC-ICR is difficult to study given that dividing cells have access to replication-coupled ICL repair. Assessing the impact of TC-ICR in isolation requires an experimental system which allows monitoring of replication independent ICL repair. Cell free and *in vitro* reporter reactivation systems have helped circumvent this hurdle. Cell free extracts from *Xenopus laevis* eggs do not undergo replication and have been used to study RIR of ICLs (4) and to identify MutSα mediated repair of ICLs via MMR machinery (5). Plasmid reporter assays have been employed to study transcription-coupled ICL repair by monitoring repair of transcription blocking lesions. Insertion of a crosslink bearing oligonucleotide between a strong promoter and a reporter gene allows measurement of transcription-coupled repair and bypass of ICLs (10,38). We have designed a fluorescence-based reporter that lacks an origin of replication, ensuring that we specifically measure transcription dependent ICL repair.

UVSSA is required for repair of a single ICL blocking transcription of a fluorophore, thus establishing UVSSA as critical for transcription-coupled repair of ICLs. We show that UVSSA localizes to damaged chromatin in cells treated with crosslinking drugs where it interacts with transcribing Pol II. Moreover, UVSSA interacts with transcription-coupled repair proteins CSA, CSB, and TFIIH upon ICL damage. Notably, loss of UVSSA-TFIIH interaction impairs transcription-coupled ICL repair. Our MS analysis of UVSSA-interacting proteins failed to identify FA proteins upon ICL damage, suggesting that TC-ICR is independent of replication-coupled ICL repair.

UVSSA: a common node in NER and TC-ICR

Analysis of SJG-136-dependant UVSSA protein interactions suggests that TC-ICR is initiated upon Pol II stalling at the ICL. CSB and CSA are then recruited to stalled Pol II and in turn recruit UVSSA. UVSSA could then target TFIIH to the lesion as is the case in NER, where its endonuclease activity initiates repair of the ICL by cleaving the transcribed DNA strand. Similar interactions have been characterized in repair of UV lesions via the TC-NER pathway (32) implying a significant degree of overlap between these repair mechanisms. In addition, we show that UVSSA interaction with TFIIH is similarly required for repair of ICL or UV lesions (21). Analysis of UVSSA interactomes by MS following UV or ICL damage reveals a strong positive correlation, indicating that similar mechanisms are activated in response to different DNA lesions. The ability of transcription-coupled repair to resolve diverse lesions is an efficient system to protect the cell from transcription stalling. Transcription-coupled repair is known to respond to a wide variety of lesions (45), and we demonstrate that that sensitivity extends to ICLs.

Translesion synthesis (TLS) polymerases are required for replication independent repair (RIR) of ICLs, possibly contributing to lesion removal during TC-ICR. In yeast, NER machinery functions in

conjunction with TLS polymerase Pol η to remove an MMC induced ICL (46). Similarly, the TLS polymerase Pol κ, which functions in NER during the gap filling step, (47) is also required for RIR of ICLs in *Xenopus* cell free extracts (4). Finally, the TLS polymerase Pol ζ has been directly implicated in TC-ICR in human cells (10). It is likely that multiple TLS and replicative polymerases are coordinated to effect lesion bypass during TC-ICR, facilitated by PCNA as observed in RIR of ICLs (4). Additionally, CSB recruitment of the exonuclease SNM1A to ICLs may facilitate lesion processing prior to TLS (48), as observed in replication-coupled ICL repair (49). Further research is needed to fully understand how TLS polymerases are recruited and coordinated with other repair proteins to effect ICL removal during TC-ICR.

TC-ICR is required for ICL survival independently of replication-coupled repair

Cells lacking UVSSA are sensitized to crosslinking drugs and show a significant delay in ICL repair. Given the role of UVSSA in TC-ICR, this strongly suggests that TC-ICR is required for cell homeostasis in response to ICL damage. While replication-coupled ICL repair is likely functional in UVSSA deficient cells, we propose that this pathway is not able to compensate for loss of TC-ICR. It may be that ICL repair by the FA pathway during replication is not sufficient to resolve all crosslink induced genotoxicity, which would suggest that replication-coupled and replication independent ICL repair mechanisms are not redundant (Fig 4). Previous studies indicate that these pathways contribute independently to ICL resistance: combined inhibition of TC-ICR and FA pathways results in additive sensitivity to crosslinking drugs (10). The sensitivity of TC-ICR defective cells to ICLs could have multiple causes. ICLs forming within essential genes may stall transcription, requiring rapid removal to resolve transcription blocks and restore homeostasis (45). In the absence of TC-ICR, stalled RNA polymerases should accumulate, increasing the frequency of collision with DNA polymerases, resulting in Replication-Transcription Conflict (RTC). RTCs are mutagenic, can cause chromosome rearrangement (50), and would occur regardless of FA pathway functionality. Alternatively, in the absence of UVSSA, TC-ICR initiates but aborts, leaving a repair intermediate that cannot be processed by replication-coupled ICL repair. A similar situation has been described following the loss of Pol κ (4). While loss of TC-ICR sensitizes cells, hyperactivation of the pathway may alleviate ICL induced transcription stalling and RTCs by increasing the efficiency of repair, promoting cellular resistance to crosslinking drugs. This could result in acquired chemoresistance, as observed in hyperactivation of other repair pathways in cancer (51) and suggested by increased ICL resistance in high UVSSA expression cancer lines.

While TC-ICR is required for survival of crosslinker treatment, it might have a modest impact on ICL repair in unstressed growth conditions. Defects in the FA pathway, involved in replication-coupled ICL repair, result in bone marrow failure and cancer predisposition, highlighting the importance of ICL repair during normal replication (1). In contrast, UVSS patients, defective in TC-NER and TC-ICR, display UV sensitivity without cancer predisposition or other developmental abnormalities (52). CSA and CSB are also likely required for TC-ICR (10) and are mutated in the TC-NER deficiency disease Cockayne syndrome (CS), characterized by developmental delay and short lifespan (18). These patients are likely also defective in TC-ICR, but the divergence in clinical presentation between UVSS and CS suggests that TC-ICR deficiency does not contribute significantly to CS phenotypes. CSA and CSB requirement for oxidative lesion repair (17) or Pol II transcription processivity (13) has been posited to explain the differences in CS and UVSS symptoms. Therefore, loss of UVSSA more specifically inhibits TC-NER and TC-ICR without compromising other transcription or repair functions, and analysis of UVSS phenotypes is the most reliable way to interpret the significance of TC-ICR for unstressed growth.

In light of this, it appears that TC-ICR might play a minor role in maintaining genome stability under physiological conditions, while FA is vital. Spontaneous ICLs are rare and transcription stalling caused by endogenous ICL damage in UVSSA deficient cells may be resolved by replication-coupled ICL

repair. Alternatively, other replication independent ICL repair mechanisms, such as MMR and GG-NER, may compensate for TC-ICR loss at physiological levels of ICL damage. The phenotypes reported in FA patients indicate that TC-ICR is unable to compensate for loss of replication-coupled ICL repair. This is not surprising, since TC-ICR only operates in the transcribed genome, leaving ICLs in non-transcribed regions unrepaired in FA deficient cells. These observations support a model in which TC-ICR is specifically required for transcription stability during times of high ICL damage, most notably following cancer chemotherapy.

Our results suggest that UVSSA and TC-ICR may be relevant to the treatment of cancer patients. Precision oncology uses genomic profiling of tumors to predict the potential therapeutic value of an intervention (53), allowing for selection of the most suited treatment for each patient. Repair protein activity is associated with cancer patient outcomes; high ERCC1 expression is linked to poor chemotherapeutic response (41,42) while deleterious mutations in NER pathway proteins correlate with improved prognosis (54). Our analysis shows that UVSSA expression correlates with resistance to crosslink inducing drugs in some cancer types, indicating that UVSSA expression may have value as a biomarker to inform chemotherapeutic choice during cancer treatment. In conclusion, our work establishes UVSSA as a factor in transcription-coupled repair of ICLs, elucidates the mechanisms through which transcription stalling initiates repair of ICLs, and reinforces the independence of TC-ICR from replication-coupled ICL repair mechanisms.

DATA AVAILABILITY

The mass spectrometry proteomics data have been deposited to the ProteomeXchange Consortium via the PRIDE (55) partner repository with the dataset identifier PXD041455.

All other data underlying this article is accessible in Dryad with DOI https://doi.org/10.5061/dryad.rfj6q57g8

SUPPLEMENTARY DATA

Supplementary Data are available at NAR online.

AUTHOR CONTRIBUTIONS

R. C. Liebau conducted the majority of experiments. C. Waters conducted initial experiments in clonogenic sensitivity, engineering of the pEm-N1-CW reporter plasmid, initial experiments in ICL repair efficiency, and helped design the sgRNA for UVSSA knockout. A. Ahmed conducted immunofluorescence microscopy experiments and analyzed the data. R.K. Soni conducted liquid chromatography and mass spectrometry with initial data analysis. R. C. Liebau, C. Water, A Ahmed, J. Gautier designed the study, analyzed data, and wrote the paper

FUNDING

This work was supported in part by National Institute of Health [grant numbers 1R35 CA197606, 1P01 CA174653 to JG]. Funding for open access charge by National Institute of Health [grant number 1P01 CA174653].

CONFLICT OF INTEREST

The authors declare no competing financial interests.

ACKNOWLEDGEMENTS

We thank Dr Ciccia (Columbia University) and lab members for providing materials and guidance to conduct iSTOP knockout. We thank Dr. Tanaka (Osaka University) for the gift of the FLAG-UVSSA

construct. We thank the Proteomics and Macromolecular Crystallography Shared Resource, Herbert Irving Comprehensive Cancer Center (HICCC) at Columbia University (National Institute of Health grant number 5P30-CA013696).

REFERENCES

1. Moldovan, G.-L. and D'Andrea, A.D. (2009) How the Fanconi Anemia pathway guards the genome. *Annual review of genetics*, **43**, 223-249.
2. Schärer, O.D. (2005) DNA Interstrand Crosslinks: Natural and Drug-Induced DNA Adducts that Induce Unique Cellular Responses. *ChemBioChem*, **6**, 27-32.
3. Williams, H.L., Gottesman, M.E. and Gautier, J. (2013) The differences between ICL repair during and outside of S-Phase. *Trends Biochem Sci*, **38**, 386-393.
4. Williams, H.L., Gottesman, M.E. and Gautier, J. (2012) Replication-Independent Repair of DNA Interstrand Crosslinks. *Mol Cell*, **47**, 140-147.
5. Kato, N., Kawasoe, Y., Williams, H., Coates, E., Roy, U., Shi, Y., Beese, L.S., Schärer, O.D., Yan, H., Gottesman, M.E. *et al.* (2017) Sensing and Processing of DNA Interstrand Crosslinks by the Mismatch Repair Pathway. *Cell Reports*, **21**, 1375-1385.
6. Muniandy, P.A., Thapa, D., Thazhathveetil, A.K., Liu, S.-t. and Seidman, M.M. (2009) Repair of Laser-localized DNA Interstrand Cross-links in G1 Phase Mammalian Cells. *The Journal of Biological Chemistry*, **284**, 27908-27917.
7. Wood, R.D. (2010) Mammalian nucleotide excision repair proteins and interstrand crosslink repair. *Environmental and Molecular Mutagenesis*, **51**, 520-526.
8. Larminat, F., Zhen, W. and Bohr, V.A. (1993) Gene-specific DNA repair of interstrand cross-links induced by chemotherapeutic agents can be preferential. *Journal of Biological Chemistry*, **268**, 2649-2654.
9. Slyskova, J., Sabatella, M., Ribeiro-Silva, C., Stok, C., Theil, A.F., Vermeulen, W. and Lans, H. (2018) Base and nucleotide excision repair facilitate resolution of platinum drugs-induced transcription blockage. *Nucleic Acids Res*, **46**, 9537-9549.
10. Enoiu, M., Jiricny, J. and Schärer, O.D. (2012) Repair of cisplatin-induced DNA interstrand crosslinks by a replication-independent pathway involving transcription-coupled repair and translesion synthesis. *Nucleic Acids Res*, **40**, 8953-8964.
11. Steurer, B. and Marteijn, J.A. (2017) Traveling Rocky Roads: The Consequences of Transcription-Blocking DNA Lesions on RNA Polymerase II. *Journal of Molecular Biology*, **429**, 3146-3155.
12. Nakazawa, Y., Hara, Y., Oka, Y., Komine, O., van den Heuvel, D., Guo, C., Daigaku, Y., Isono, M., He, Y., Shimada, M. *et al.* (2020) Ubiquitination of DNA Damage-Stalled RNAPII Promotes Transcription-Coupled Repair. *Cell*, **180**, 1228-1244.e1224.
13. Kokic, G., Wagner, F.R., Chernev, A., Urlaub, H. and Cramer, P. (2021) Structural basis of human transcription–DNA repair coupling. *Nature*, **598**, 368.
14. Marteijn, J.A., Lans, H., Vermeulen, W. and Hoeijmakers, J.H.J. (2014) Understanding nucleotide excision repair and its roles in cancer and ageing. *Nature Reviews Molecular Cell Biology*, **15**, 465-481.
15. Nieto Moreno, N., Olthof, A.M. and Svejstrup, J.Q. (2023) Transcription-Coupled Nucleotide Excision Repair and the Transcriptional Response to UV-Induced DNA Damage. *Annual Review of Biochemistry*, **92**, null.
16. Lehmann, A.R., McGibbon, D. and Stefanini, M. (2011) Xeroderma pigmentosum. *Orphanet Journal of Rare Diseases*, **6**, 70.
17. Spivak, G. (2005) UV-sensitive syndrome. *Mutation Research/Fundamental and Molecular Mechanisms of Mutagenesis*, **577**, 162-169.
18. Karikkineth, A.C., Scheibye-Knudsen, M., Fivenson, E., Croteau, D.L. and Bohr, V.A. (2017) Cockayne syndrome: Clinical features, model systems and pathways. *Ageing Research Reviews*, **33**, 3-17.

19. Zhang, X., Horibata, K., Saijo, M., Ishigami, C., Ukai, A., Kanno, S.-i., Tahara, H., Neilan, E.G., Honma, M., Nohmi, T. *et al.* (2012) Mutations in UVSSA cause UV-sensitive syndrome and destabilize ERCC6 in transcription-coupled DNA repair. *Nat Genet*, **44**, 593-597.
20. Higa, M., Zhang, X., Tanaka, K. and Saijo, M. (2016) Stabilization of Ultraviolet (UV)-stimulated Scaffold Protein A by Interaction with Ubiquitin-specific Peptidase 7 Is Essential for Transcription-coupled Nucleotide Excision Repair. *The Journal of Biological Chemistry*, **291**, 13771-13779.
21. Okuda, M., Nakazawa, Y., Guo, C., Ogi, T. and Nishimura, Y. (2017) Common TFIIH recruitment mechanism in global genome and transcription-coupled repair subpathways. *Nucleic Acids Res*, **45**, 13043-13055.
22. Sato, M., Liebau, A.W., Liu, Z., Liu, L., Rabadan, R. and Gautier, J. (2021) The UVSSA complex alleviates MYC-driven transcription stress. *Journal of Cell Biology*, **220**.
23. Oshima, K., Zhao, J., Pérez-Durán, P., Brown, J.A., Patiño-Galindo, J.A., Chu, T., Quinn, A., Gunning, T., Belver, L., Ambesi-Impiombato, A. *et al.* (2020) Mutational and functional genetics mapping of chemotherapy resistance mechanisms in relapsed acute lymphoblastic leukemia. *Nature Cancer*, **1**, 1113-1127.
24. Adeyemi, R.O., Willis, N.A., Elia, A.E.H., Clairmont, C., Li, S., Wu, X., D'Andrea, A.D., Scully, R. and Elledge, S.J. (2021) The Protexin complex counters resection on stalled forks to promote homologous recombination and crosslink repair. *Molecular Cell*, **81**, 4440-4456.e4447.
25. Kulak, N.A., Pichler, G., Paron, I., Nagaraj, N. and Mann, M. (2014) Minimal, encapsulated proteomic-sample processing applied to copy-number estimation in eukaryotic cells. *Nat Methods*, **11**, 319-324.
26. Meier, F., Brunner, A.-D., Koch, S., Koch, H., Lubeck, M., Krause, M., Goedecke, N., Decker, J., Kosinski, T., Park, M.A. *et al.* (2018) Online Parallel Accumulation–Serial Fragmentation (PASEF) with a Novel Trapped Ion Mobility Mass Spectrometer. *Molecular & Cellular Proteomics : MCP*, **17**, 2534-2545.
27. Cox, J., Neuhauser, N., Michalski, A., Scheltema, R.A., Olsen, J.V. and Mann, M. (2011) Andromeda: A Peptide Search Engine Integrated into the MaxQuant Environment. *Journal of Proteome Research*, **10**, 1794-1805.
28. Billon, P., Bryant, E.E., Joseph, S.A., Nambiar, T.S., Hayward, S.B., Rothstein, R. and Ciccia, A. (2017) CRISPR-Mediated Base Editing Enables Efficient Disruption of Eukaryotic Genes through Induction of STOP Codons. *Mol Cell*, **67**, 1068-1079.e1064.
29. Tyanova, S., Temu, T., Sinitcyn, P., Carlson, A., Hein, M.Y., Geiger, T., Mann, M. and Cox, J. (2016) The Perseus computational platform for comprehensive analysis of (prote)omics data. *Nat Methods*, **13**, 731-740.
30. Schindelin, J., Arganda-Carreras, I., Frise, E., Kaynig, V., Longair, M., Pietzsch, T., Preibisch, S., Rueden, C., Saalfeld, S., Schmid, B. *et al.* (2012) Fiji: an open-source platform for biological-image analysis. *Nat Methods*, **9**, 676-682.
31. Schwertman, P., Lagarou, A., Dekkers, D.H.W., Raams, A., van der Hoek, A.C., Laffeber, C., Hoeijmakers, J.H.J., Demmers, J.A.A., Fousteri, M., Vermeulen, W. *et al.* (2012) UV-sensitive syndrome protein UVSSA recruits USP7 to regulate transcription-coupled repair. *Nat Genet*, **44**, 598-602.
32. van der Weegen, Y., Golan-Berman, H., Mevissen, T.E.T., Apelt, K., González-Prieto, R., Goedhart, J., Heilbrun, E.E., Vertegaal, A.C.O., van den Heuvel, D., Walter, J.C. *et al.* (2020) The cooperative action of CSB, CSA, and UVSSA target TFIIH to DNA damage-stalled RNA polymerase II. *Nature Communications*, **11**, 2104.
33. Balajee, A.S. and Geard, C.R. (2004) Replication protein A and gamma-H2AX foci assembly is triggered by cellular response to DNA double-strand breaks. *Exp Cell Res*, **300**, 320-334.
34. Wang, A.T., Sengerová, B., Cattell, E., Inagawa, T., Hartley, J.M., Kiakos, K., Burgess-Brown, N.A., Swift, L.P., Enzlin, J.H., Schofield, C.J. *et al.* (2011) Human SNM1A and XPF-ERCC1 collaborate to initiate DNA interstrand cross-link repair. *Genes Dev*, **25**, 1859-1870.

35. Klein Douwel, D., Hoogenboom, W.S., Boonen, R.A. and Knipscheer, P. (2017) Recruitment and positioning determine the specific role of the XPF-ERCC1 endonuclease in interstrand crosslink repair. *EMBO J*, **36**, 2034-2046.
36. Klein Douwel, D., Boonen, R.A.C.M., Long, D.T., Szypowska, A.A., Räschle, M., Walter, J.C. and Knipscheer, P. (2014) XPF-ERCC1 acts in Unhooking DNA interstrand crosslinks in cooperation with FANCD2 and FANCP/SLX4. *Mol Cell*, **54**, 460-471.
37. Pepper, C.J., Hambly, R.M., Fegan, C.D., Delavault, P. and Thurston, D.E. (2004) The Novel Sequence-Specific DNA Cross-Linking Agent SJG-136 (NSC 694501) Has Potent and Selective In vitro Cytotoxicity in Human B-Cell Chronic Lymphocytic Leukemia Cells with Evidence of a p53-Independent Mechanism of Cell Kill. *Cancer Research*, **64**, 6750-6755.
38. Ang, W.H., Myint, M. and Lippard, S.J. (2010) Transcription inhibition by platinum-DNA cross-links in live mammalian cells. *Journal of the American Chemical Society*, **132**, 7429-7435.
39. Hirose, Y. and Ohkuma, Y. (2007) Phosphorylation of the C-terminal Domain of RNA Polymerase II Plays Central Roles in the Integrated Events of Eucaryotic Gene Expression. *The Journal of Biochemistry*, **141**, 601-608.
40. Fei, J. and Chen, J. (2012) KIAA1530 Protein Is Recruited by Cockayne Syndrome Complementation Group Protein A (CSA) to Participate in Transcription-coupled Repair (TCR). *Journal of Biological Chemistry*, **287**, 35118-35126.
41. Kwon, H.C., Roh, M.S., Oh, S.Y., Kim, S.H., Kim, M.C., Kim, J.S. and Kim, H.J. (2007) Prognostic value of expression of ERCC1, thymidylate synthase, and glutathione S-transferase P1 for 5-fluorouracil/oxaliplatin chemotherapy in advanced gastric cancer. *Annals of Oncology: Official Journal of the European Society for Medical Oncology*, **18**, 504-509.
42. Kirschner, K. and Melton, D.W. (2010) Multiple Roles of the ERCC1-XPF Endonuclease in DNA Repair and Resistance to Anticancer Drugs. *Anticancer Research*, **30**, 3223-3232.
43. Deans, A.J. and West, S.C. (2011) DNA interstrand crosslink repair and cancer. *Nat Rev Cancer*, **11**, 467-480.
44. Chatterjee, N. and Walker, G.C. (2017) Mechanisms of DNA damage, repair, and mutagenesis. *Environmental and Molecular Mutagenesis*, **58**, 235-263.
45. Lans, H., Hoeijmakers, J.H.J., Vermeulen, W. and Marteijn, J.A. (2019) The DNA damage response to transcription stress. *Nature Reviews Molecular Cell Biology*, **20**, 766-784.
46. Zheng, H., Wang, X., Warren, A.J., Legerski, R.J., Nairn, R.S., Hamilton, J.W. and Li, L. (2003) Nucleotide excision repair- and polymerase η-mediated error-prone removal of mitomycin C interstrand cross-links. *Molecular and Cellular Biology*, **23**, 754-761.
47. Ogi, T. and Lehmann, A.R. (2006) The Y-family DNA polymerase κ (pol κ) functions in mammalian nucleotide-excision repair. *Nature Cell Biology*, **8**, 640-642.
48. Iyama, T., Lee, S.Y., Berquist, B.R., Gileadi, O., Bohr, V.A., Seidman, M.M., McHugh, P.J. and Wilson, D.M. (2015) CSB interacts with SNM1A and promotes DNA interstrand crosslink processing. *Nucleic Acids Res*, **43**, 247-258.
49. Baddock, H.T., Yosaatmadja, Y., Newman, J.A., Schofield, C.J., Gileadi, O. and McHugh, P.J. (2020) The SNM1A DNA repair nuclease. *DNA Repair*, **95**, 102941.
50. St Germain, C., Zhao, H. and Barlow, J.H. (2021) Transcription-Replication Collisions—A Series of Unfortunate Events. *Biomolecules*, **11**, 1249.
51. Sakthivel, K.M. and Hariharan, S. (2017) Regulatory players of DNA damage repair mechanisms: Role in Cancer Chemoresistance. *Biomedicine & Pharmacotherapy*, **93**, 1238-1245.
52. Schwertman, P., Vermeulen, W. and Marteijn, J.A. (2013) UVSSA and USP7, a new couple in transcription-coupled DNA repair. *Chromosoma*, **122**, 275-284.
53. Schwartzberg, L., Kim, E.S., Liu, D. and Schrag, D. (2017) Precision Oncology: Who, How, What, When, and When Not? *American Society of Clinical Oncology Educational Book*, 160-169.

54. Ceccaldi, R., O'Connor, K.W., Mouw, K.W., Li, A.Y., Matulonis, U.A., D'Andrea, A.D. and Konstantinopoulos, P.A. (2015) A Unique Subset of Epithelial Ovarian Cancers with Platinum Sensitivity and PARP Inhibitor Resistance. *Cancer research*, **75**, 628-634.
55. Perez-Riverol, Y., Bai, J., Bandla, C., García-Seisdedos, D., Hewapathirana, S., Kamatchinathan, S., Kundu, Deepti J., Prakash, A., Frericks-Zipper, A., Eisenacher, M. *et al.* (2022) The PRIDE database resources in 2022: a hub for mass spectrometry-based proteomics evidences. *Nucleic Acids Res*, **50**, D543-D552.

TABLE AND FIGURES LEGENDS

Figure 1

A

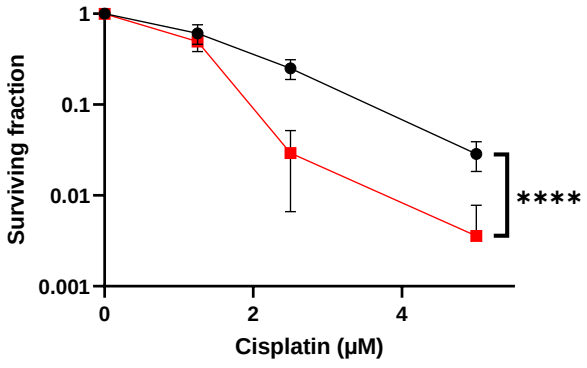

B

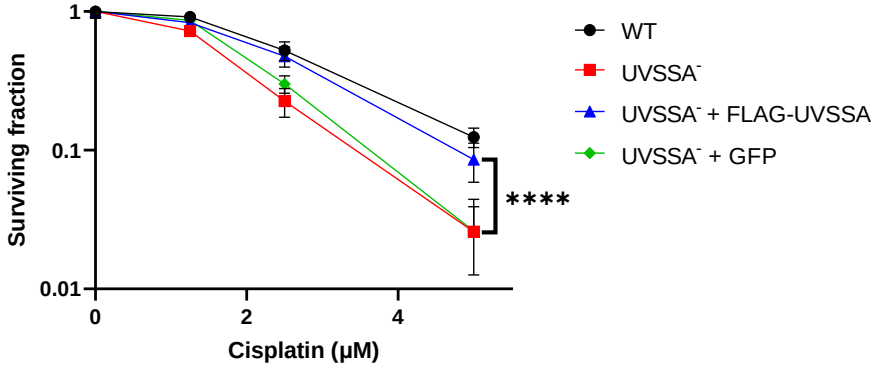

C

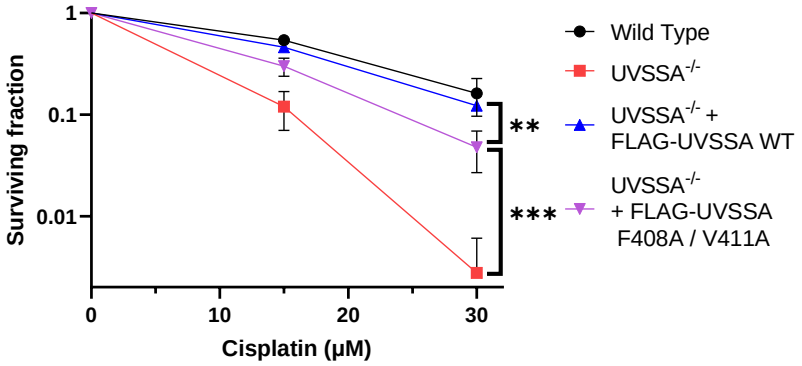

D

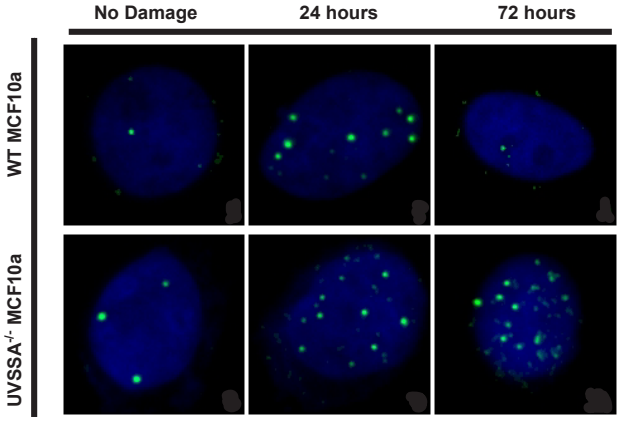

E

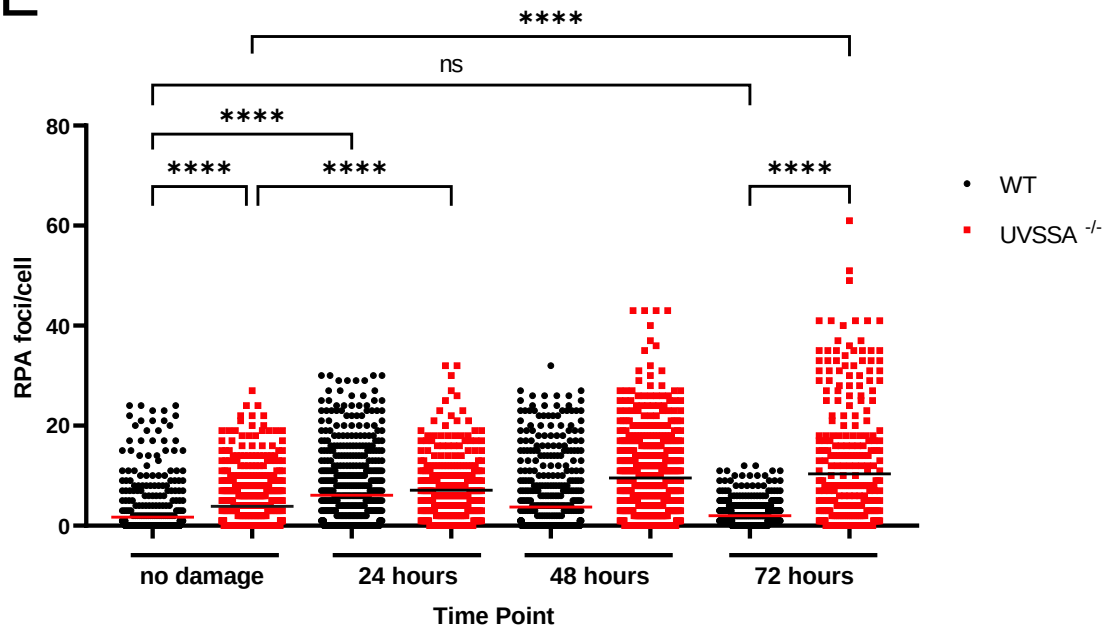

Figure 1 UVSSA deficient cells are sensitive to cisplatin
A) Clonogenic assays monitoring WT and UVSSA^{-} Hap-1 cell survival after 4-hour cisplatin exposure at the indicated doses. **B)** Same as in (A) for WT, UVSSA^{-}, UVSSA^{-} expressing GFP, and UVSSA^{-} expressing FLAG-UVSSA WT Hap-1 cells. **C)** Same as in (A) for WT, UVSSA$^{-/-}$, UVSSA$^{-/-}$ expressing FLAG-UVSSA WT, and UVSSA$^{-/-}$ expressing FLAG-UVSSA F408A/ V411A MCF10a cells. For A-C, N=6, data is mean and SD of biological replicates. Statistical analysis by two tailed *t*-test, ** $p<0.01$, *** $p<.001$, **** $P<0.0001$. **D)** Representative images of immunofluorescence microscopy monitoring RPA Foci at 24-hour intervals in WT and UVSSA$^{-/-}$ MCF10a cells treated with 20nM SJG-136 for 1 hour. RPA foci are shown in green stained by anti RPA antibody. The nucleus is shown in blue by DAPI staining. **E)** Quantification of RPA foci per cell in MCF10a cells treated as described in (D). Mean is indicated by a solid line. For each column left to right N= 644, 651, 570, 305, 621, 552, 843, 327. Statistical analysis by one way ANOVA with multiple comparisons, **** $p<0.0001$

Figure 2

A

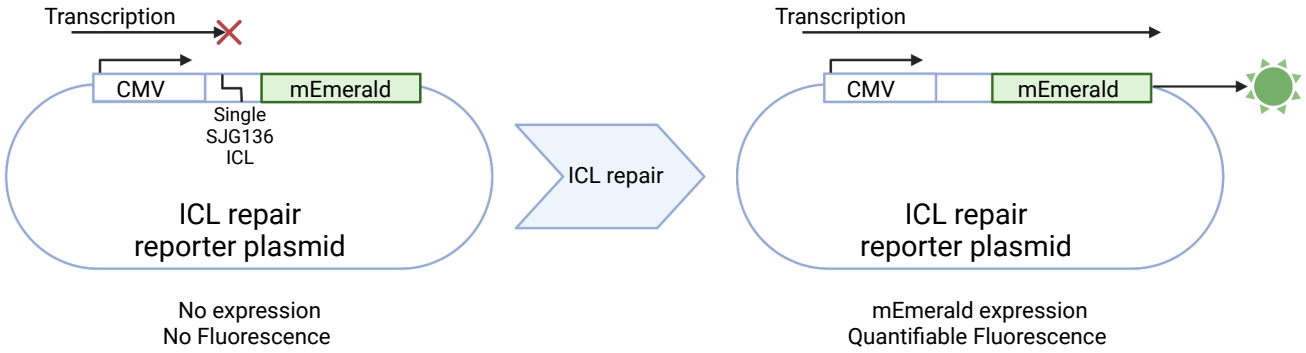
Transcription
CMV
mEmerald
Single
SJG136
ICL
ICL repair
reporter plasmid
No expression
No Fluorescence
ICL repair
Transcription
CMV
mEmerald
ICL repair
reporter plasmid
mEmerald expression
Quantifiable Fluorescence

B

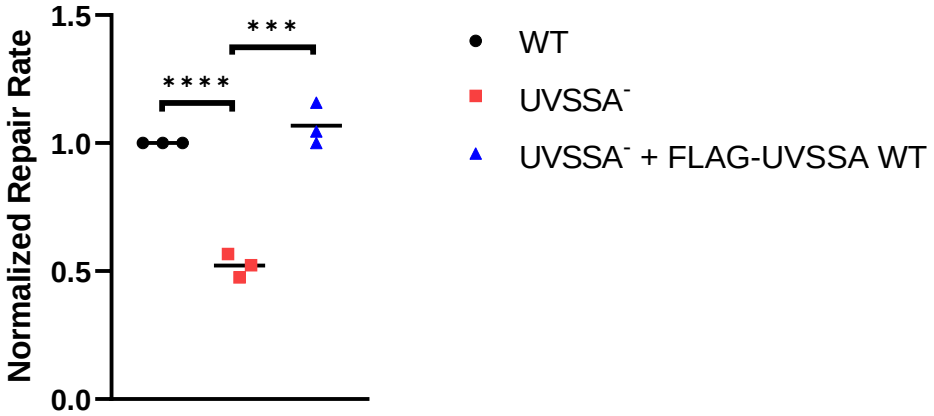
Normalized Repair Rate
1.5
1.0
0.5
0.0
****
***
WT
UVSSA-
UVSSA- + FLAG-UVSSA WT

C

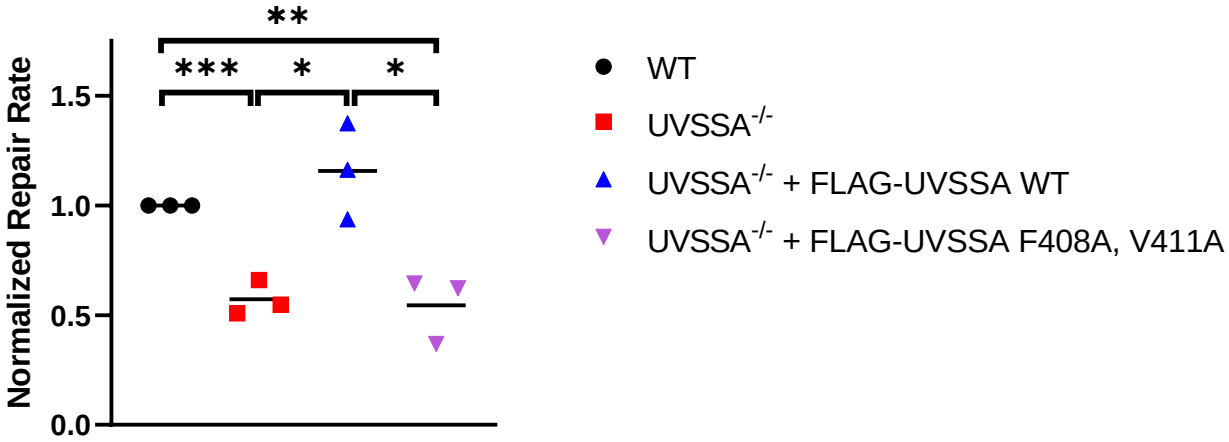
Normalized Repair Rate
1.5
1.0
0.5
0.0
**
***
*
*
WT
UVSSA-/-
UVSSA-/- + FLAG-UVSSA WT
UVSSA-/- + FLAG-UVSSA F408A, V411A

Figure 2 UVSSA is required for transcription-coupled repair of a single ICL
A) Diagram of the reporter plasmid used to monitor transcription-coupled ICL repair. A crosslink bearing oligonucleotide is inserted between a strong promoter and an mEmerald coding region. When transfected into cells, the ICL prevents transcription progression until it is repaired, resulting in mEmerald expression and cell fluorescence. Created using Biorender.com. **B)** Normalized ICL repair efficiency in WT, UVSSA^{-} and UVSSA^{-} expressing FLAG-UVSSA Hap-1 lines transfected with the ICL reporter. N=3 independent experiments, mean is indicated. **C)** Normalized ICL repair efficiency in WT, UVSSA$^{-/-}$, UVSSA$^{-/-}$ expressing FLAG-UVSSA WT and UVSSA$^{-/-}$ expressing FLAG-UVSSA F408A/ V411A MCF10a lines transfected with the ICL reporter. N=3 independent experiments, mean is indicated. For panels B and C, repair rates are normalized to WT repair rate for each independent experiment. Statistical analysis by two tailed *t*-test, * p <0.05, ** p <0.01, *** p <0.001, **** p <0.0001

Figure 3

A

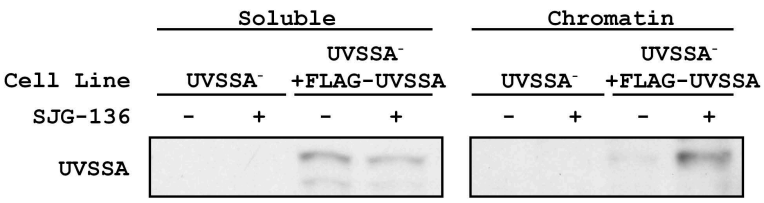

B

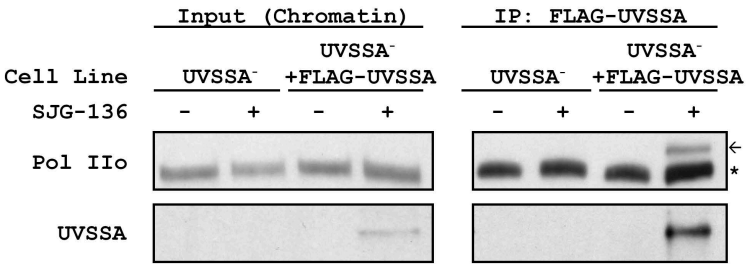

E

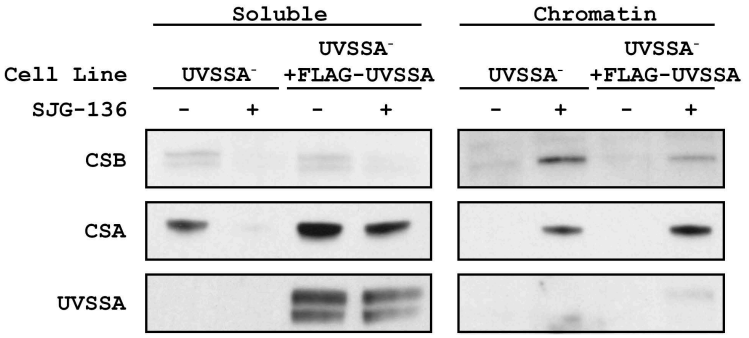

F

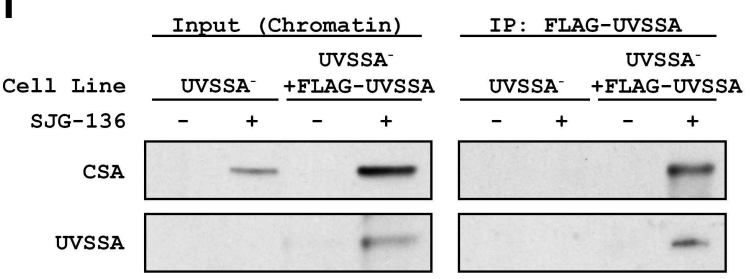

C

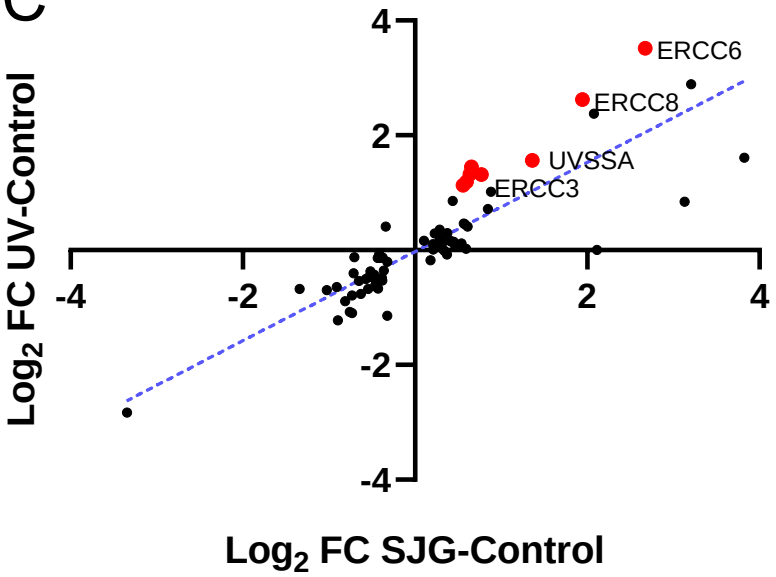

D

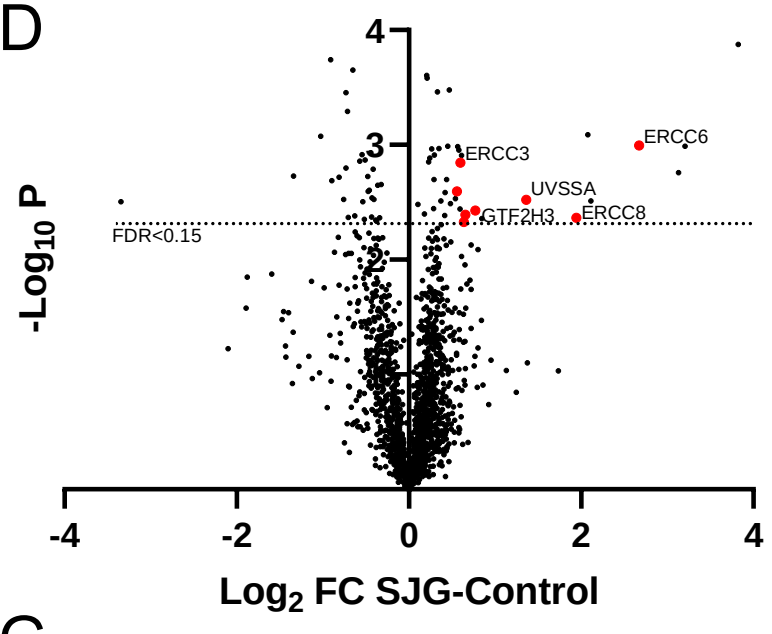

G

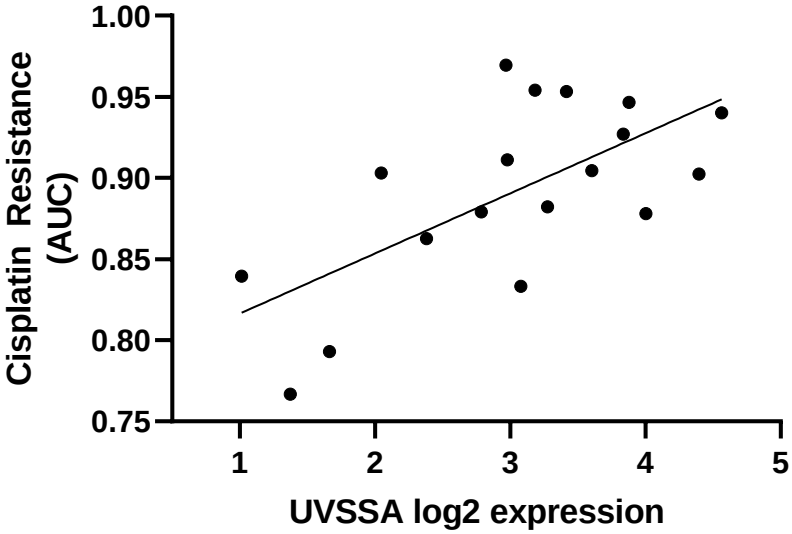

Figure 3 UVSSA localizes to ICL-damaged chromatin and interacts with transcription and repair proteins upon ICL damage

A) FLAG-UVSSA localization following cell fractionation in UVSSA$^-$ and UVSSA$^-$ expressing FLAG-UVSSA Hap-1 cells treated with 100nM SJG-136 for two hours. Quantification of biological replicates shown in Fig S3A. **B)** Input and FLAG immunoprecipitation from chromatin fractions of UVSSA$^-$ and UVSSA$^-$ expressing FLAG-UVSSA Hap-1 cells treated with 100nM SJG-136 for two hours. Blots were probed with UVSSA antibody and an antibody specific for the elongating form of Pol II: Pol IIo. Arrow indicates a Pol II band that specifically interacts with UVSSA upon DNA damage, * indicates a nonspecific band. Quantification of biological replicates shown in Fig S3B. This figure represents a composite of multiple representative western blots. **C)** FLAG-UVSSA expressing Hap-1 cells treated with 100nM SJG-136 for 2 hours or exposed to 20 J/m^2 UV-C were fractionated, and chromatin fractions were subjected to FLAG immunoprecipitation followed by mass spectrometry (see Methods). Comparison of protein enrichment in this data set is shown. Proteins significantly enriched by an FDR threshold of 0.15 are displayed. Proteins with previously characterized repair function are highlighted in red. Log_2 fold change (log_2 FC) upon SJG-136 treatment is plotted on the X axis, while log_2 FC upon UV damage is plotted on the Y axis. A linear regression is depicted by the dashed line, $P<0.0001$, N=74. **D)** Volcano plot showing protein enrichment in FLAG-UVSSA pulldown from Hap-1 cell chromatin fractions following 100nM SJG-136 treatment for 2 hours. Log2 FC upon SJG-136 treatment is plotted on the X axis, while the *p* value of enrichment (two tailed t-test) is plotted on the Y axis. Repair proteins are highlighted in red, based on an FDR threshold of 0.15. **E)** Same as (A) western blots were probed with CSA, CSB, and UVSSA antibodies. This figure represents a composite of multiple representative western blots. Quantification of biological replicates shown in Fig S3D, E. **F)** Same as (B), western blots were probed with CSA and UVSSA antibodies. This figure represents a composite of multiple representative western blots. For all western blots in this figure, no editing was conducted besides rotation of the entire image to ensure proper orientation. **G)** Correlation between UVSSA expression (RNA-seq) on the X axis and cisplatin resistance (Area Under the Curve) on the Y axis in Acute Lymphocytic Leukemia lines. Data was accessed from the Depmap Portal, Expression 22Q2 and Sanger GDSC1 data sets, respectively. Linear regression analysis is depicted by a solid line, $p = 0.0027$, N=18

Wildtype

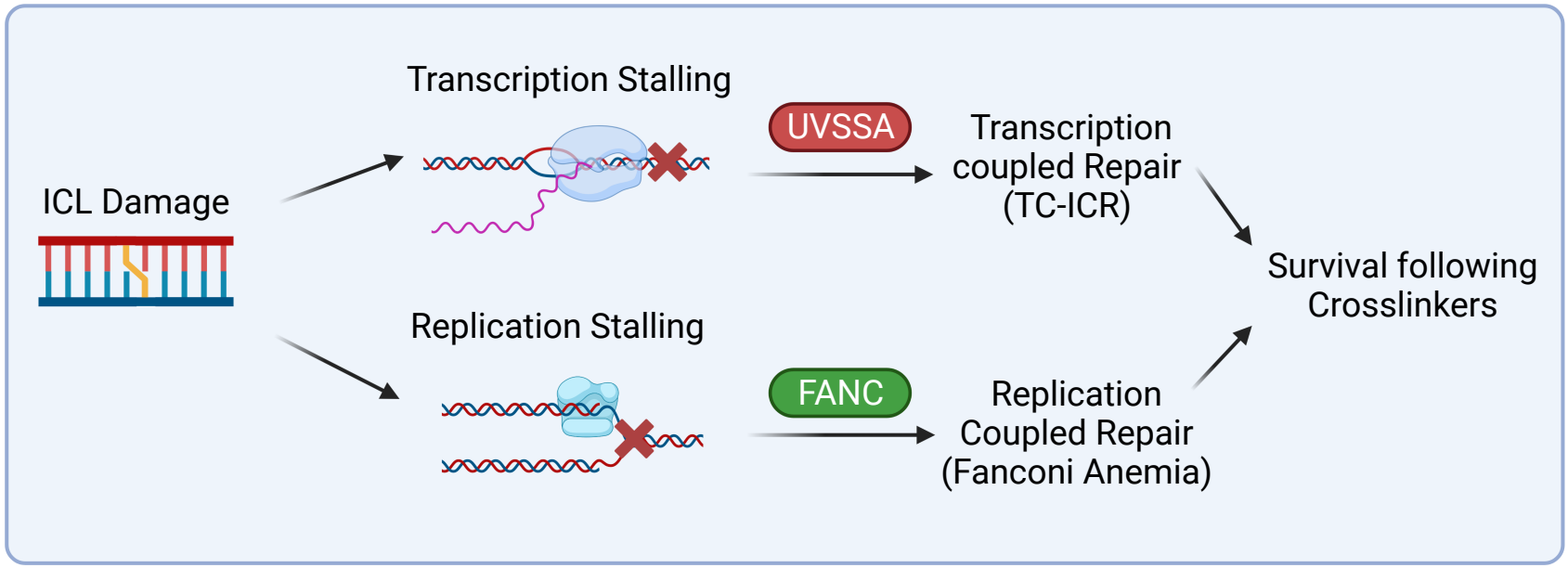

UVSSA knockout

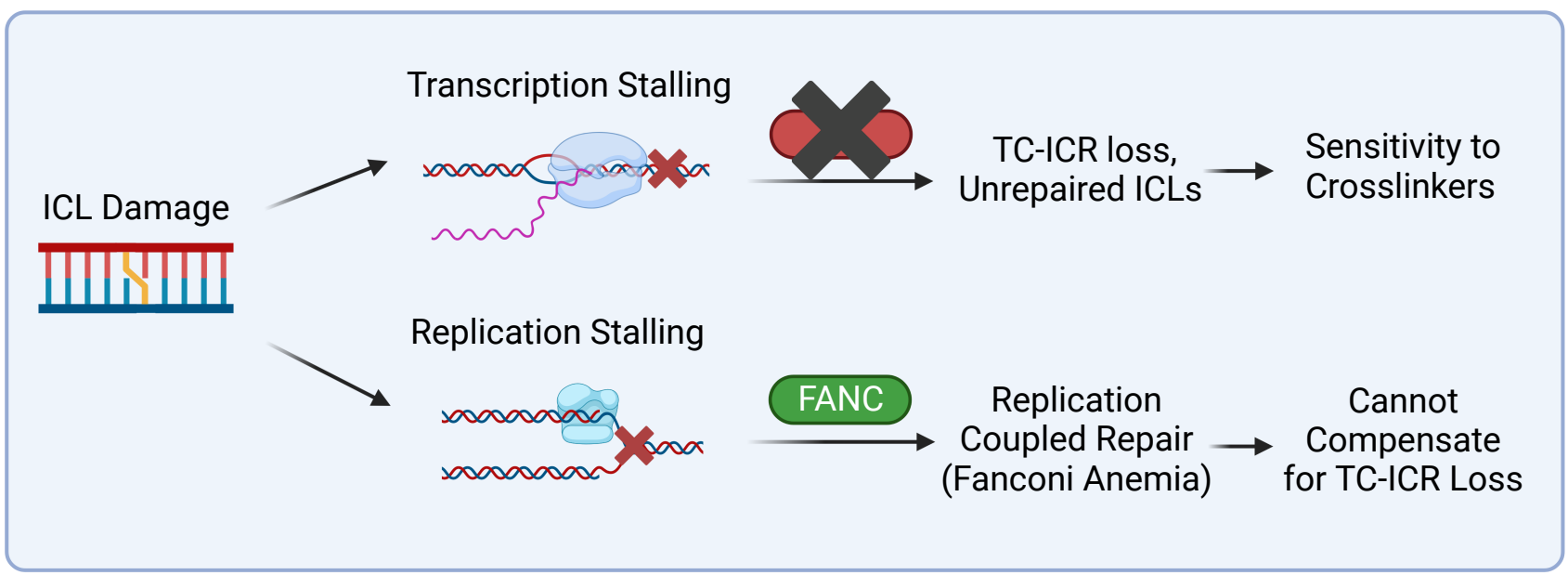

Figure 4 Contribution of replication and transcription-coupled repair in survival following crosslink inducing drug treatment in wildtype and UVSSA knockout cells

Diagram depicting the contributions of replication and transcription-coupled repair mechanisms to survival from crosslinking drugs. Chemotherapeutics induce ICLs that cause stalling of both transcription and replication machinery, requiring TC-ICR and Fanconi Anemia pathways to resolve these genotoxic stresses, respectively. These pathways function independently to promote the survival of crosslinker treated cells. The repair protein UVSSA is essential for TC-ICR, and cells lacking UVSSA are sensitized to crosslink inducing drugs. Replication-coupled ICL repair mechanisms are unable to compensate for the loss of TC-ICR, further supporting the independence of these pathways. Created using Biorender.com

Cell Type	Drug	Slope	Pearson	P value linear regression
ALL	Cisplatin	12.5	0.701	9.25e-4
ALL	Mitomycin C	3.3	0.491	5.35e-2
Esophagus	Cisplatin	7.66	0.399	3.91e-2
Breast Ductal Carcinoma	Cisplatin	12.2	0.62	4.65e-3
Breast Ductal Carcinoma	Mitomycin C	1.9	0.453	2.61e-2

Table 1 Crosslinking chemotherapy resistance and UVSSA expression levels are correlated in several cancer types

Table of cancer types displaying a significant correlation between crosslinking drug resistance and UVSSA expression in the depmap database (Sanger GDSC1 and Expression 22Q1 data sets, respectively). Slope, Pearson correlation, and *p* values were generated by linear regression analysis using the depmap web portal (https://depmap.org/portal/)